Spatial Carrierless Amplitude and Phase Modulation Technique for Visible Light Communication Systems

Spatial Carrierless Amplitude and Phase Modulation Technique for Visible Light Communication Systems

Kabiru O. Akande, *Student Member, IEEE,* and Wasiu O. Popoola, *Senior Member, IEEE*

***Abstract*—Spatial carrierless amplitude and phase modulation (S-CAP) technique is developed in this paper as a physical layer solution to improve the spectral efficiency of the conventional CAP scheme while preserving its low complexity transceiver design. The S-CAP technique is proposed and investigated for systems employing the visible light communication (VLC) technology. An analytical expression for the joint detection of the spatial and signal bits for the user equipment (UE) experiencing line-of-sight propagation (LOS) is derived and validated via simulation. The effect of multipath propagation and user mobility on the bit-error-rate (BER) performance of the proposed S-CAP are also investigated. It is found that the (BER) performance of S-CAP in LOS is dictated by the minimum of the channel gains $h_{\min}$, the signal constellation points (SCP) and the channel gain dissimilarity, $\Delta|h|$. The power factor imbalance (PFI) and multiple photodetectors (PDs) are then introduced to improve performance and mitigate channel impairments. The use of PFI and PDs in LOS result in signal-to-noise (SNR) gain of 33.5 dB and 43 dB, respectively. The proposed scheme is thus a novel implementation of CAP in a multiple-input multiple-output (MIMO) system and demonstrates its potential as a suitable physical layer solution for VLC technology.**

***Index Terms*—Multiple-input multiple-output (MIMO), visible light communication (VLC), spatial modulation (SM), carrierless amplitude and phase modulation (CAP), multipath propagation.**

I. Introduction

Visible light communication (VLC) is an emerging technology that employs existing lighting fixtures to realise high-speed data communication links [1, 2]. It has been proposed as a complementary communication technology to radio frequency (RF) in some applications due to its potential to offer high data rate to existing wireless communication infrastructure. The IEEE 802.15 wireless personal area network task group has completed standards for both the physical (PHY) and medium access control (MAC) layer of VLC technology [3]. A revision task group has also been commissioned to expand the VLC standard into infrared, near ultraviolet wavelengths and optical camera communications [4]. The numerous benefits of VLC include huge unlicensed spectrum, power efficient and inexpensive devices, high security and immunity to electromagnetic interference, among others [2, 5].

The bandlimited light emitting diodes (LEDs) used in VLC together with the intensity modulated and direct detection (IM/DD) technique require spectrally-efficient modulation schemes, whose transmitted signals are real, unipolar and non-negative. Advanced modulation schemes such as pulse amplitude modulation (PAM) and orthogonal frequency division multiplexing (OFDM) have been employed to realise efficient, high data rate transmission in the Gb/s range [6, 7]. In addition, carrierless amplitude and phase modulation (CAP) has also been proposed as an efficient modulation scheme in VLC systems with a data rate of up to 8 Gb/s [8]. The CAP scheme is a high-dimensional, low-complexity modulation format with the ability to transmit data symbols in parallel. The transmitted symbols are separated at the receiver using digital orthogonal waveforms which result in a simpler and low-complexity implementation for CAP. Recent progress has seen CAP implemented as a multiband scheme (m-CAP) with improved tolerance towards the non-linearity effect of the VLC channel [9, 10]. The improved performance of m-CAP has also been experimentally verified and demonstrated for VLC links [11].

Much of the work reported in the literature focuses on designing equalization techniques to improve the achievable data rate of CAP [8, 12]. These techniques lead to a significant increase in the complexity of the resulting system. Therefore, in this paper, a spatial modulation-based CAP (S-CAP) is proposed to improve the spectral efficiency of CAP while maintaining its low complexity. During each symbol duration, only one LED transmits data out of N_{t}. This 'active' LED transmits the CAP signal. With S-CAP, additional information bits are encoded on the location (or index) of the transmitting LED. That is, an extra $\log_2(N_{\mathrm{t}})$ information bits are encoded on the index of the transmitting LED. Thus, by transmitting extra bits in the spatial domain, S-CAP achieves higher throughput compared to the conventional CAP. The benefits of S-CAP can be illustrated in two ways: (*i*) for a fixed number of transmitted bits/symbol, S-CAP requires lower bandwidth in comparison to CAP. (*ii*) For a fixed bandwidth requirement, S-CAP transmits more bits/symbol thus achieving a higher spectral efficiency. For a bit duration T_{b} and modulation order M, the S-CAP symbol duration can be expressed as:

$$T_{\text{S-CAP}} = T_{\mathrm{b}} \log_2 M N_{\mathrm{t}} \tag{1}$$

while CAP symbol duration is expressed as:

$$T_{\text{CAP}} = T_{\mathrm{b}} \log_2 M \tag{2}$$

Using (1) and (2), the spectral efficiency improvement factor of S-CAP over the conventional CAP can be derived as:

$$\eta_f = \frac{T_{\text{S-CAP}}}{T_{\text{CAP}}} = \log_M (M N_{\mathrm{t}}) \tag{3}$$

Thus, the proposed S-CAP is a low-complexity MIMO technique that enhances the spectral efficiency of CAP-based VLC systems.

Manuscript received April 15, 2018.

The authors are with the LiFi Research and Development Centre, School of Engineering, Institute for Digital Communications, The University of Edinburgh, Edinburgh EH9 3JL, U.K. (e-mail: {K.Akande,W.Popoola}@ed.ac.uk).

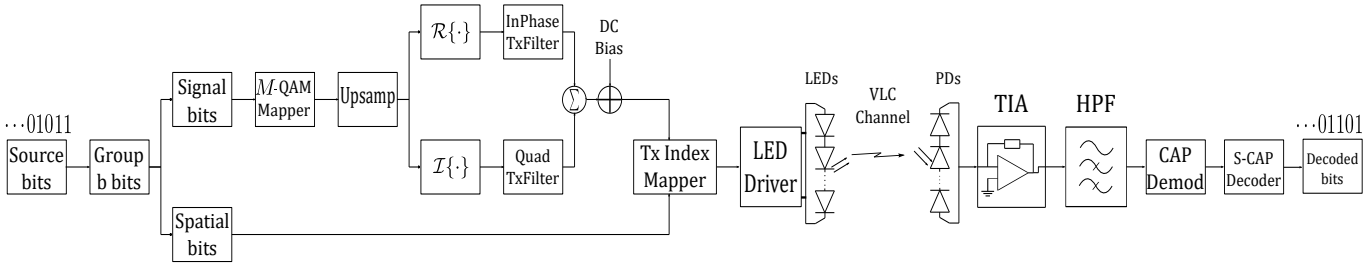

Fig. 1. The schematic block diagram of the proposed S-CAP transceiver for VLC link.

A. Related Work

Multiple LEDs are often deployed in VLC in order to meet the required illumination level due to the limited luminous flux of a single LED. This feature has been exploited in literature to realise various MIMO techniques [13–15]. Recently, theoretical analysis and experimental demonstrations of the benefits of MIMO techniques (spatial multiplexing and repetitive coding) have been reported for the CAP modulation technique [16, 17]. Another MIMO transmission technique that has been studied in optical wireless communication is the spatial modulation (SM). Only one out of N_t LEDs is active at any instant in an SM system. The index/position of this active LED is then used to encode data [18, 19]. In SM, a block of information bits to be transmitted is divided into two subblocks. One subblock is mapped to symbols in the signal domain corresponding to the regular modulation scheme while the other is used to activate one of the LED transmitters in the spatial domain. Therefore, the signal domain bits are transmitted through the activated LED while other LEDs remain inactive [20]. Unlike spatial multiplexing, the SM technique avoids inter-carrier/inter-channel interference at the receiver while improving the spectral efficiency of the system. The SM technique has been studied and compared with other modulation schemes in [13, 14]. Experimental demonstrations of SM techniques have also been reported for optical wireless systems in [21]. These studies conclude that SM offers a low complexity approach to improving the throughput of optical wireless communication systems.

B. Contributions and Organization of this work

The specific contributions of this paper are highlighted as follows:

- S-CAP is proposed as a low-complexity, spectrally-efficient modulation scheme for VLC indoor applications;
- analytical expression for the error performance of S-CAP is derived and verified through simulation;
- the effect of multipath propagation and user mobility on the error performance of S-CAP is investigated using the ray-tracing channel model; and
- power factor imbalance (PFI) and multiple PDs are investigated as techniques for improving the error performance of the proposed S-CAP scheme.

The rest of the paper is organized as follows: the S-CAP system model is presented in Section II while the BER expression for S-CAP is derived in Section III. Section IV contains the simulation results and discussions while Section V concludes the paper.

TABLE I
S-CAP MAPPING ILLUSTRATION, $N_t = 2$ AND $M = 4$.

Input b bits	LED index	Signal constellation
000	1	$+1 + j$
001	1	$-1 + j$
010	1	$-1 - j$
011	1	$+1 - j$
100	2	$+1 + j$
101	2	$-1 + j$
110	2	$-1 - j$
111	2	$+1 - j$

II. S-CAP System Model

The block diagram illustrating the modulation process of S-CAP is shown in Fig. 1. The stream of information bits is grouped into blocks of b bits, where $b = \log_2(N_t) + \log_2(M)$. The $\log_2(N_t)$ bits is taken as the spatial bits and mapped to a transmitter index while the remaining $\log_2(M)$ bits, taken as the signal bits, is passed to the CAP modulator. The signal bits are mapped to the corresponding M-QAM symbol, upsampled to match the system sampling rate and separated into real and imaginary part before being fed into the transmit filters. The real and imaginary part of the transmit filters are orthogonal and are generated by multiplying the root raised cosine filter (RRC) with $\cos(\omega_c t)$ and $\sin(\omega_c t)$, respectively [10]. A suitable DC bias is added to the summation of the filters' output to make the real-valued signal non-negative and suitable for the intensity modulation of the optical carrier. In order to select the appropriate transmitter, the $\log_2(N_t)$ spatial bits are mapped to an index which corresponds to one of the available N_t transmitting LEDs.

The mapping process for the proposed S-CAP is illustrated in Table I for the case of $N_t = 2$ and $M = 4$. Starting with the most significant bit (MSB), $\log_2(N_t)$ bits are mapped to the LED index to activate the transmitter while the remaining $\log_2(M)$ bits are mapped to the CAP signal amplitude to be sent on the activated transmitter. For example, when the input bits is 011, the MSB '0′ is mapped to the LED1 while the remaining bits '11′ are mapped to the signal symbol $+1 - j$

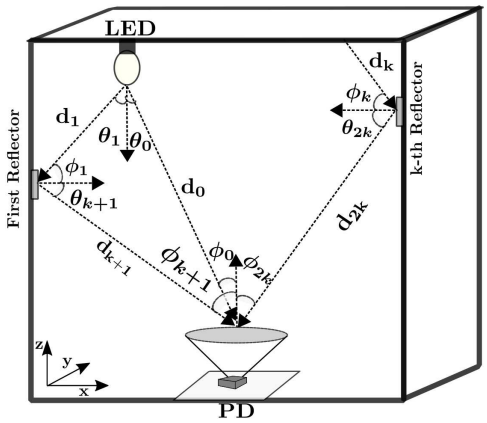

Fig. 2. The path profile for the ray tracing indoor optical wireless channel model.

where +1 and −1 become the amplitudes of the in-phase and quadrature filters, respectively. The transmitted optical signal from the LED, $s(t)$, can thus be represented as:

$$s(t) = \eta(\beta x(t) + x_{\mathrm{dc}}) \tag{4}$$

where η is the electrical to optical conversion coefficient while β represents the optical modulation index. The CAP modulated signal, $x(t)$ is expressed as:

$$x(t) = \sum_{n=-\infty}^{\infty} [a_n p(t - nT) - b_n \bar{p}(t - nT)] \tag{5}$$

where

$$p(t) = g(t)\cos(\omega_c t) \tag{6}$$

and

$$\bar{p}(t) = g(t)\sin(\omega_c t) \tag{7}$$

are the pair of real and imaginary transmit orthogonal filters, $g(t)$ is the pulse-shaping RRC, T is the symbol duration and $\omega_c = 2\pi f_c$ is the center frequency of the CAP signal spectrum and is of the same order as T. The DC bias, x_{dc}, is added to the signal to make it unipolar and avoid any clipping distortion. The average emitted optical power from the LED can be obtained from (4) as $P = \underset{\forall t}{\mathbb{E}}\{s(t)\}$ where $\mathbb{E}\{\cdot\}$ is the expectation operator.

After traversing the optical channel with a fixed LOS configuration and path loss h, the received electrical signal at the output of the PIN photodiode detector (PD), with the DC component suppressed, is given by:

$$y(t) = \Re h\eta\beta x(t) + n(t) \tag{8}$$

where $\Re$ is the responsivity of the photodetector and $n(t)$ is the sum of ambient and thermal noise at the receiver. The noise is modelled as independent and identically distributed additive white Gaussian noise (AWGN) with zero-mean and double-sided power spectral density, $N_0/2$. The electrical signal is then passed through the CAP demodulator and S-CAP decoder to jointly detect the LED index and the corresponding data symbol bits.

III. BER Performance Analysis for S-CAP

Considering an arbitrary $N_{\mathrm{r}} \times N_{\mathrm{t}}$ MIMO configuration, the received signal in (8) can now be expressed as :

$$\mathbf{y} = \Re\eta\beta\mathbf{H}\mathbf{x} + \mathbf{n} \tag{9}$$

where $\mathbf{y}$ is an $N_{\mathrm{r}} \times 1$ received signal vector, $\mathbf{H}$ is the $N_{\mathrm{r}} \times N_{\mathrm{t}}$ channel matrix with component $h_{n_{\mathrm{r}}n_{\mathrm{t}}}$ representing the channel gain from the n_{t}th transmitter to the n_{r}th receiver, $\mathbf{x}$ is an $N_{\mathrm{t}} \times 1$ transmitted vector and $\mathbf{n}$ is an $N_{\mathrm{r}} \times 1$ noise components. The received signal on the n_{r}th receiver given that symbol m has been transmitted on the n_{t}th transmitter is then written as:

$$y_{n_{\mathrm{r}}}(t) = r^m_{n_{\mathrm{r}}n_{\mathrm{t}}}(t) + n_{n_{\mathrm{r}}}(t) \qquad n_{\mathrm{r}} = 1, 2, \cdots, N_{\mathrm{r}} \tag{10}$$

where $r^m_{n_{\mathrm{r}}n_{\mathrm{t}}}(t) = \Re\eta\beta h_{n_{\mathrm{r}}n_{\mathrm{t}}} x_m(t)$. At each receiver, the S-CAP demodulator uses a pair of linear filters that are, respectively, matched to the pair of the transmit orthogonal filters. From (10), the output of the CAP demodulators can be expressed as:

$$\mathbf{y} = \mathbf{r}^m_{n_{\mathrm{t}}} + \mathbf{n} \tag{11}$$

where $y_{n_{\mathrm{r}}}$, $r^m_{n_{\mathrm{r}}n_{\mathrm{t}}}$ and $n_{n_{\mathrm{r}}}$ are the components of $\mathbf{y}$, $\mathbf{r}^m_{n_{\mathrm{t}}}$ and $\mathbf{n}$, respectively. The S-CAP detector will then make a decision on the transmitted signal in each signal interval based on the demodulator output such that the probability of a correct decision is maximized. Assuming perfect synchronization and full knowledge of the channel matrix $\mathbf{H}$, the S-CAP optimum detector employs Maximum Likelihood (ML) criterion since $\{x_m\}_{m=1}^{M}$ are equiprobable with $p(x_m) = 1/M$. Thus, the S-CAP optimum detector decides on the $x_{mn_{\mathrm{t}}}$, which is the mth symbol transmitted on the n_{t}th transmitter, that maximizes the probability density function (PDF) of $\mathbf{y}$ conditioned on $\mathbf{r}^m_{n_{\mathrm{t}}}$ as:

$$\hat{x}_{mn_{\mathrm{t}}} = \arg\max_{n_{\mathrm{t}},m} p(\mathbf{y}|\mathbf{r}^m_{n_{\mathrm{t}}}) \tag{12}$$

where the conditional PDF, given the AWGN corrupted channel, is expressed as:

$$p(\mathbf{y}|\mathbf{r}^m_{n_{\mathrm{t}}}) = \frac{1}{(2\pi N_0)^{N_{\mathrm{r}}/2}} \exp\left[-\sum_{n_{\mathrm{r}}=1}^{N_{\mathrm{r}}} \frac{\left|y_{n_{\mathrm{r}}} - r^m_{n_{\mathrm{r}}n_{\mathrm{t}}}\right|^2}{2N_0}\right] \tag{13}$$

The ML criterion reduces to finding the $x_{mn_{\mathrm{t}}}$ that results in the minimum Euclidean distance, i.e.

$$\hat{x}_{mn_{\mathrm{t}}} = \arg\min_{n_{\mathrm{t}},m} D(\mathbf{y}, \mathbf{r}^m_{n_{\mathrm{t}}}) \tag{14}$$

and the distance metrics is given by:

$$D(\mathbf{y}, \mathbf{r}^m_{n_{\mathrm{t}}}) = \sum_{n_{\mathrm{r}}=1}^{N_{\mathrm{r}}} \left|y_{n_{\mathrm{r}}} - r^m_{n_{\mathrm{r}}n_{\mathrm{t}}}\right|^2 \tag{15}$$

To find the error probability of S-CAP, we consider a joint detection of both the transmitter index and the transmitted symbol using pairwise error probability, PEP. The PEP of S-CAP is defined as the probability that the S-CAP detector decides in favour of vector $\tilde{\mathbf{x}}$ given that $\mathbf{x}$ has actually been transmitted. If the detector makes the correct decision, the decision metrics become

$$D(\mathbf{y}, \mathbf{r}^m_{n_{\mathrm{t}}}) = \sum_{n_{\mathrm{r}}=1}^{N_{\mathrm{r}}} \left|n_{n_{\mathrm{r}}}\right|^2 \tag{16}$$

$$\mathrm{BER}_{\text{S-CAP}} \leq \frac{1}{MN_{\mathrm{t}}\log_2(MN_{\mathrm{t}})}\sum_{m=1}^{M}\sum_{n_t=1}^{N_{\mathrm{t}}}\sum_{\tilde{m}=1}^{M}\sum_{\tilde{n}_{\mathrm{t}}=1}^{N_{\mathrm{t}}}\mathcal{N}_H(\tilde{b}_{mn_t}, b_{mn_{\mathrm{t}}})Q\left(\sqrt{\frac{(\Re\beta\eta)^2T}{2N_0}\sum_{n_{\mathrm{r}}=1}^{N_{\mathrm{r}}}\left|x_m h_{n_{\mathrm{r}}n_t} - x_{\tilde{m}}h_{n_{\mathrm{r}}\tilde{n}_{\mathrm{t}}}\right|^2}\right). \tag{16}$$

TABLE II
CONFIGURATION PARAMETERS FOR THE CHANNEL MODELLING.

Parameter	Value	Parameter	Value
LED half angle, $\varphi_{1/2}$	60°	ρ_{ceiling}	0.48
Field of view of PD	85°	ρ_{floor}	0.63
Temporal resolution : Δt	0.2 ns	ρ_{wall}	0.83
Spatial resolution : ΔA_{PD}	0.04 m^2	PD area, A_{PD}	1 cm^2

otherwise,

$$D(\mathbf{y}, \tilde{\mathbf{r}}^m_{n_{\mathrm{t}}}) = \sum_{n_{\mathrm{r}}=1}^{N_{\mathrm{r}}}\left|r^m_{n_{\mathrm{r}}n_{\mathrm{t}}} - \tilde{r}^m_{n_{\mathrm{r}}n_{\mathrm{t}}} + n_{n_{\mathrm{r}}}\right|^2 \tag{17}$$

Thus, the PEP for S-CAP can be obtained as:

$$\begin{aligned}\mathrm{PEP}_{\text{S-CAP}} &= p(\mathbf{x} \rightarrow \tilde{\mathbf{x}}|\mathbf{H}) \\ &= p(D(\mathbf{y}, \mathbf{r}^m_{n_{\mathrm{t}}}) > D(\mathbf{y}, \tilde{\mathbf{r}}^m_{n_{\mathrm{t}}})) \\ &= Q\left(\sqrt{\frac{(\Re\beta\eta)^2T}{2N_0}\sum_{n_{\mathrm{r}}=1}^{N_{\mathrm{r}}}\left|x_m h_{n_{\mathrm{r}}n_t} - x_{\tilde{m}}h_{n_{\mathrm{r}}\tilde{n}_{\mathrm{t}}}\right|^2}\right). \end{aligned}\tag{18}$$

The BER performance of S-CAP can be derived from (18) by considering all possible MN_{t} signal combinations and using the union bound technique [22]. Hence, the BER of S-CAP is upper-bounded as shown in (16) where $\mathcal{N}_H(\tilde{b}_{mn_t}, b_{mn_{\mathrm{t}}})$ is the number of bit in error when the receiver decides for the symbol $\tilde{x}_{mn_t}$ instead of the transmitted symbol $x_{mn_{\mathrm{t}}}$. Alternatively, $\mathcal{N}_H(\tilde{b}_{mn_t}, b_{mn_{\mathrm{t}}})$ refers to the number of positions in which the bits corresponding to symbol $\tilde{x}_{mn_t}$ and $x_{mn_{\mathrm{t}}}$ differ (Hamming distance). For example, if a symbol corresponding to bits '100' is transmitted and the S-CAP detector erroneously detect the symbol corresponding to bits '000', '001' or '011', the $\mathcal{N}_H(\tilde{b}_{mn_t}, b_{mn_{\mathrm{t}}})$ term becomes 1, 2 or 3, respectively.

IV. Simulation Results and Discussions

In the results presented in this section, the electrical signal-to-noise ratio per bit is defined as $\gamma_b = \frac{(\Re\beta\eta)^2T}{\log_2(N_{\mathrm{t}}M)N_0}$ where $(R\beta\eta)^2T$ denotes the average transmitted electrical energy per symbol, E_s with $\mathbb{E}_{\forall t}\{x^2(t)\} = 1$.

The impulse response of the indoor optical channel is obtained using the ray-tracing algorithm reported in [23, 24]. The simulation is carried out by considering four LED positions whose coordinates, along with other simulation parameters, are given in Table II. It can be seen from Table II that the LEDs' coordinates have been chosen to realize a symmetrical arrangement. The path profile for the ray-tracing algorithm for an LED and PD is depicted in Fig. 2 while the channel impulse response (CIR) simulation procedure is detailed in [23]. The angle of incidence and irradiance are denoted by ϕ_k and θ_k, respectively while d_k represents the path traced out by the optical radiation from the source to its destination. The room dimension is configured to be 5 m in length and width (along x- and y- axis) and 3 m in height (along z-axis) but can be extended to any arbitrary dimension. The PD receiver position is varied across the dimension of the room floor to account for user mobility. Typical values of the reflectivity, ρ, adopted for the surfaces of the room in the simulation are reported in [25]. The z-axis coordinate for both LEDs and PDs have been fixed at 3 m and 0 m as they are considered attached to the ceiling and floor of the room, respectively. As a result, only the x and y coordinates are reported for the PDs. In the LOS channel simulation, the channel gain values are normalized such that the $\max\{h_{n_{\mathrm{r}}n_{\mathrm{t}}}\} = 1$ and $\min\{h_{n_{\mathrm{r}}n_{\mathrm{t}}}\} = h_{\min}$. The coordinates of all the PDs employed in the simulation, along with their configurations, are given in Table III. Some of the PDs' configurations could be considered for applications and scenarios such as video conferencing.

TABLE III
COORDINATES OF THE PDs AND LEDs EMPLOYED IN THE SIMULATIONS.

Figure	PD1	PD2	PD3	PD4	LED
Fig. 5	(0.8, 3.2)	×	×	×	1 – 4
Fig. 6	(0.8, 3.2)	(0.8, 0.8)	(3.2, 3.2)	(3.2, 0.8)	1 – 4
Fig. 10	(0.8, 2.6)	(0.8, 0.8)	(2.6, 2.6)	(2.6, 0.8)	1 & 4
Fig. 11	(0.8, 4.2)	(0.8, 0.8)	(4.2, 4.2)	(4.2, 0.8)	1 & 4
Fig. 16	(1.0, 1.0)	×	×	×	1 & 4
Fig. 17	(2.6, 2.6)	×	×	×	1 & 4
Fig. 18 (C)	(1.0, 1.0)	(3.0, 1.4)	(1.4, 3.0)	(2.0, 2.6)	1 & 4
Fig. 18 (D)	(2.6, 2.6)	(3.0, 1.4)	(1.4, 3.0)	(2.0, 2.6)	1 & 4
TX coordinates (m)	LED1 - (1.25,1.25,3), LED2 - (1.25,3.75,3), LED3 - (3.75,1.25,3), LED4 - (3.75,3.75,3)				
PD arrangement	1 PD ≙ PD1;	2 PDs ≙ PD1 & PD4;		4 PDs ≙ All PDs.	

The spectral efficiency/bandwidth improvement, η_f, provided by S-CAP over the conventional CAP is illustrated in Fig. 3 using the derived expression in (3). Furthermore, Fig. 4 shows the BER performance comparison and spectral/power efficiency trade-off of the two schemes for the same constellation order. Compared to CAP at the same constellation order, S-CAP achieves a higher spectral efficiency but its power efficiency is lower. For example, to achieve the same BER of 10^{-4} as CAP–4 with $M = 4$, S-CAP4 incurs a 6 dB power penalty but transmits an extra 1 bit/symbol which results in a spectral efficiency improvement factor of 1.5. This trend is also observed for $M = 16$ and 64. The power penalty incurred by S-CAP is due to its distinct channel gains requirement and the penalty can be substantially reduced by performance-enhancing techniques which are presented in later results.

The derived analytical expression for S-CAP is validated in Fig. 5 for different M and multiple LEDs. The figure shows that at the lower BER region where meaningful communication can be established, the derived expression shows excellent

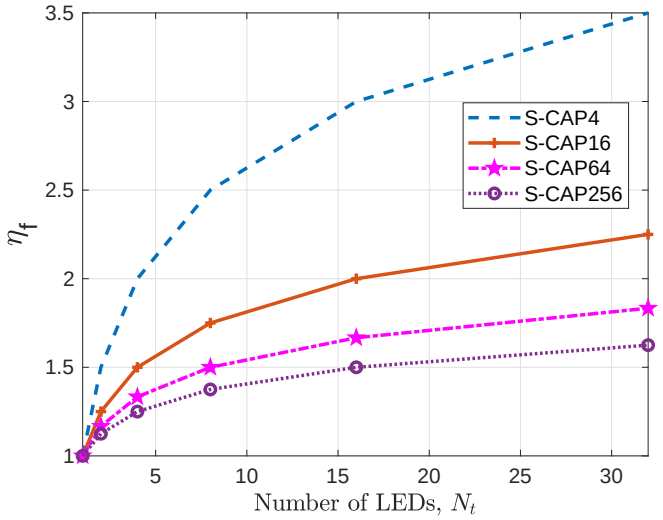

Fig. 3. Spectral efficiency improvement of S-CAP over the conventional CAP scheme for different number of LEDs and constellation sizes.

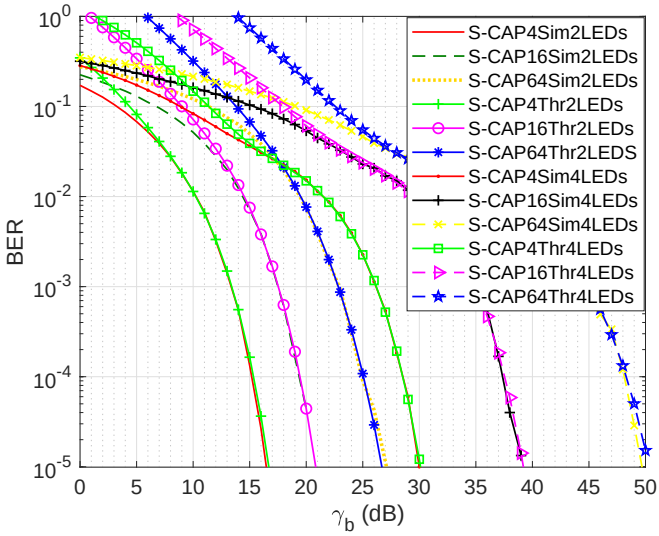

Fig. 5. BER performance comparison of S-CAP using simulation and the derived analytical expression for multiple LEDs and one PD with LOS channel gain. Sim: Simulation and Thr: Analysis

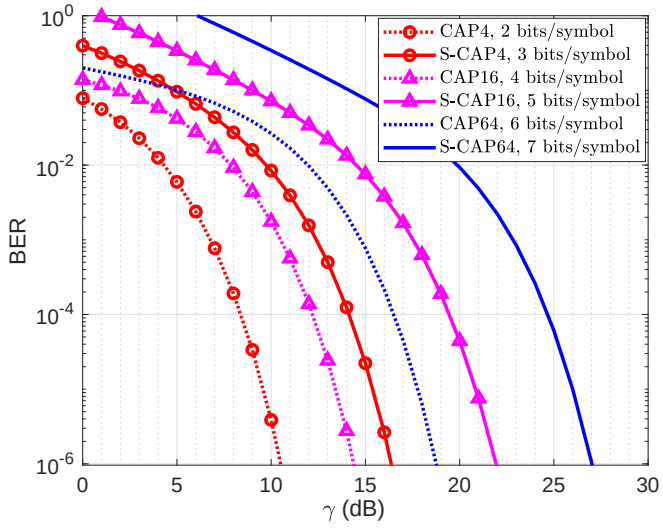

Fig. 4. Spectral/power efficiency trade-off of S-CAP compared to CAP for the same constellation order using two transmitting LEDs and one PD.

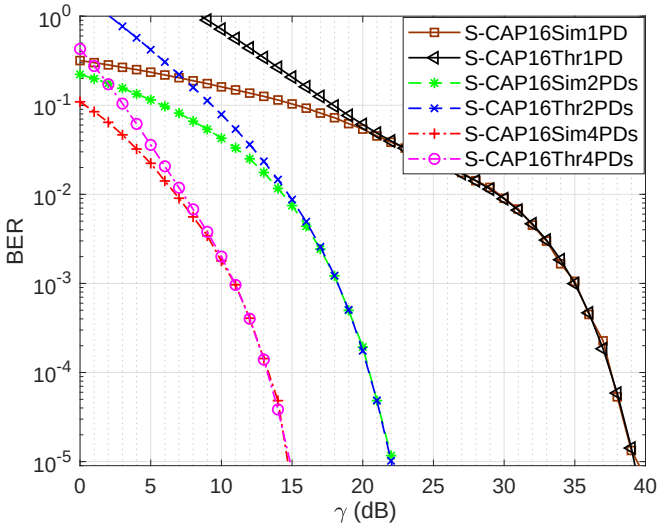

Fig. 6. BER performance comparison of S-CAP16 using simulation and the derived analytical expression for four LEDs and varying number of PDs with LOS channel gain. Sim: Simulation and Thr: Analysis

agreement with the simulation results in LOS propagation. The slight deviation at the high BER region is however due to the union bound technique considered in the analysis. The results of Fig. 5 also depicts the BER performance comparison of S-CAP for different constellation sizes. For example, it is shown that for $M = 4, 16$ and 64 and using 2 LEDs, S-CAPM requires γ_b of 15 dB, 19 dB and 25 dB, respectively to achieve a representative BER of 10^{-4}. This γ_b increases to 28 dB, 37.5 dB and 48 dB respectively in the case of four LEDs. This shows that, at the BER and PD location considered, S-CAP4, S-CAP16 and S-CAP64 respectively requires a power penalty of 13 dB, 18.5 dB and 23 dB for a corresponding increase of 33.3%, 20% and 14.1% in spectral efficiency. This illustration depicts the trade-off between the power and spectral efficiency of an S-CAP system. Henceforth, as a result of the validation, only S-CAP16 is used for further investigation.

Figure 6 shows the performance of S-CAP16 in LOS propagation using multiple LEDs and PDs (MIMO). The result confirms the tightness of the derived analytical upper bound for MIMO S-CAP. The effectiveness of using multiple PDs to improve performance, which is exploited in later results, is also reflected. In comparison to the performance of one PD, the use of two and four PDs result in γ_b improvement of 17 dB and 24 dB, respectively at a representative BER of 10^{-4}.

The γ_b required for S-CAP LOS propagation to achieve a BER of 10^{-4} at each PD location across the room is presented in Fig. 7 using two LEDs. The corresponding values of $h_{\min}$ is shown in Fig. 8. For the case of the two LEDs considered, $\{h_{n_t}\}_{n_t=1}^{N_t} = \begin{bmatrix} 1 & h_{\min} \end{bmatrix}$. In addition to the effect of γ_b, the

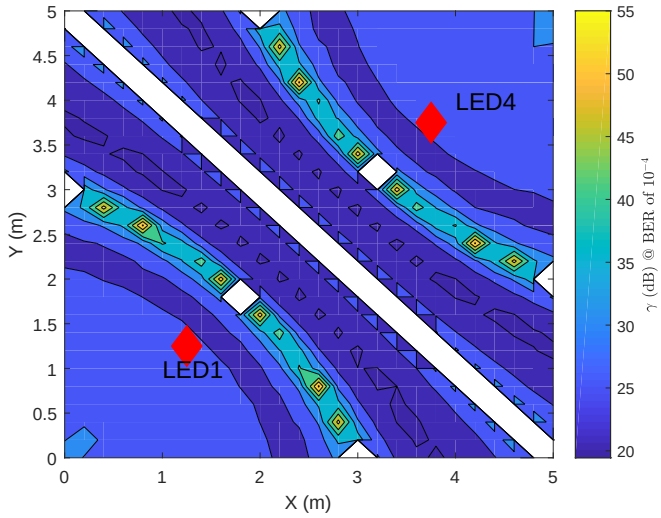

Fig. 7. The required γ_b for S-CAP16 LOS propagation to achieve BER of 10^{-4} at each PD location across the room using LED1 and LED4 whose positions are shown by the red stars. The white region shows area of BER $> 10^{-4}$.

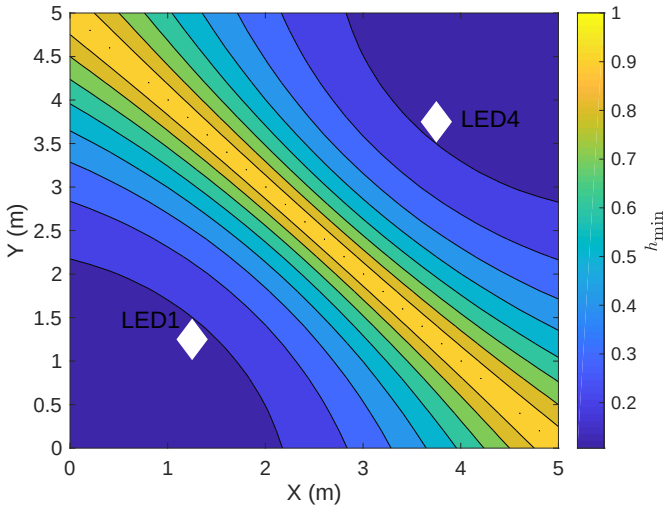

Fig. 8. Distribution of $h_{\min}$ across the room for S-CAP16 considering LED1 and LED4 whose positions are shown by the white stars.

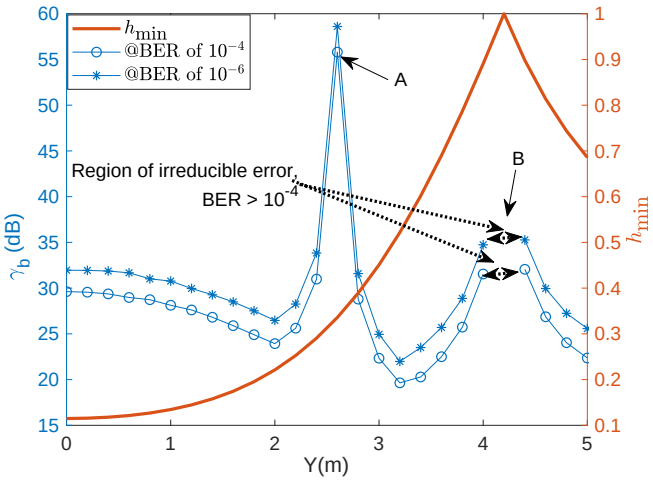

Fig. 9. SNR per bit penalty for S-CAP16 LOS propagation using LED1 and LED4 by considering a fixed location on x-axis ($x = 0.8$ m) and varying the PD's location across the y-axis overlaid by the corresponding $h_{\min}$ values.

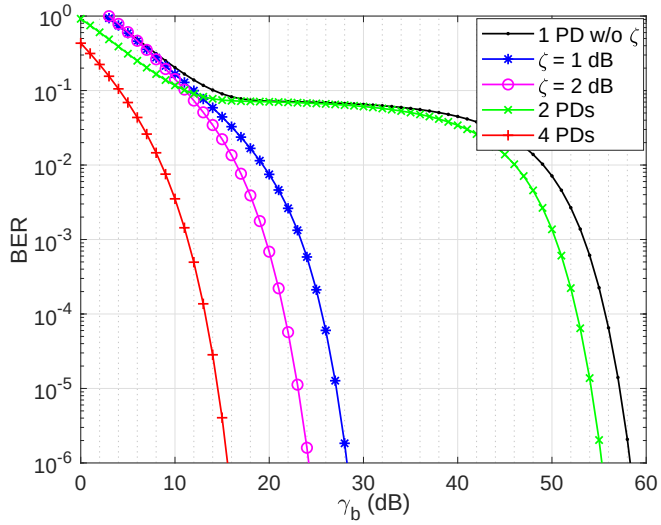

Fig. 10. Improving the BER performance of S-CAP16 through power redistribution with PFI and the use of multiple PDs at Location A in Fig. 9.

performance of S-CAP depends on the interaction of three factors. These are: (i) signal constellation points (SCP); (ii) the channel dissimilarity, ($|\Delta h|$); and (iii) the minimum value of the channel gains ($h_{\min}$). This is evident from the expression in (16). At low values of $h_{\min}$ in the range $0 \leq Y(m) \leq 2$, the required γ_b is moderate despite the fact that the channel gains are completely dissimilar ($|\Delta h| \rightarrow 1$). This means the performance is solely dictated by the small value of $h_{\min}$. Hence, as $h_{\min}$ increases the required γ_b reduces. However, the required γ_b momentarily becomes high in the range $2 < Y(m) < 2.8$ as SCP becomes the dominating factor. Beyond the range of SCP influence, $h_{\min}$ value continues to dictate the performance until $|\Delta h|$ becomes the dominating factor where $0.9 \leq h_{\min} \leq 1$ and $|\Delta h| \rightarrow 0$. Within this range, the channel gains become perfectly identical leading to an irreducible BER region.

In order to further highlight the effect of the performance-determining factors, a 2−D plot is extracted from Fig. 7 by fixing the value on x-axis at 0.8 m and varying the PD position across the y-axis. The resulting plot, overlaid by the plot of $h_{\min}$ across the same region, is depicted in Fig. 9. Within the range of $0 \leq Y(m) \leq 2$, as the value of $h_{\min}$ increases from 0.1 to 0.22, the required γ_b decreases which shows an improving performance as the BER in this region is dictated by the increasing value of $h_{\min}$. However, SCP becomes the determining factor within the range of $2 < Y(m) < 2.8$ even though the value of $h_{\min}$ continue to increase from 0.22 to 0.35. The increasing value of $h_{\min}$ together with high $|\Delta h|$ should lead to performance improvement but SCP dictates the performance degradation in this range. This explains the high γ_b at location A which

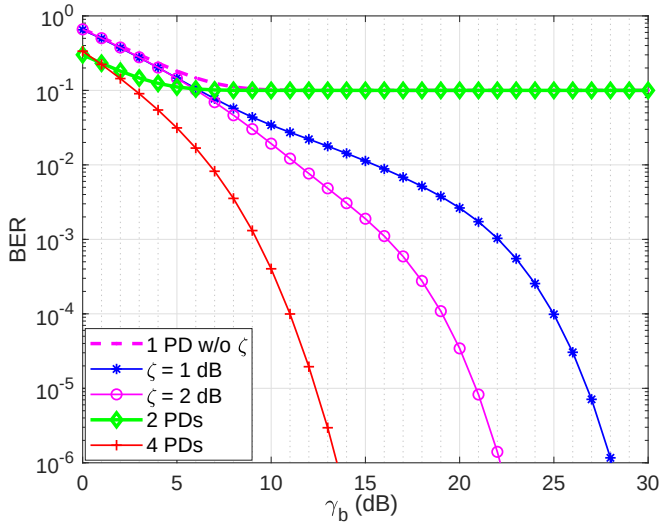

Fig. 11. Improving the BER performance of S-CAP16 through power redistribution with PFI and the use of multiple PDs at location *B* in Fig. 9.

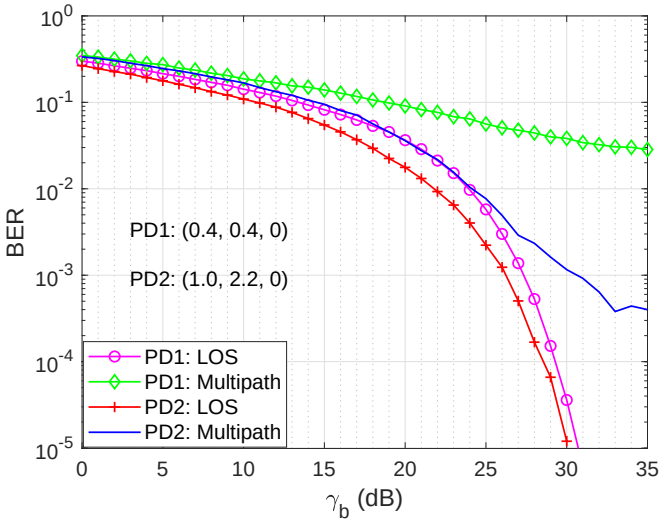

Fig. 12. Comparison of the BER performance of S-CAP16 in LOS and multipath indoor optical communication.

requires 24 dB more than the neighbouring locations to achieve the same BER of 10^{-4}. Finally, the effect of channel gains dissimilarity can be seen from the range $3.2 < Y(m) < 4.4$ where $|\Delta h| \to 0$ as the value of $h_{\min}$ increases from 0.52 to 1. At location B, where both channel gains have a value of unity ($|\Delta h| = 0$) and are thus perfectly identical, the decoder is unable to differentiate between symbols from the two LEDs. The same pattern is also recorded at lower BER of 10^{-6}.

Similar to other SM techniques, the performance of S-CAP is affected by the aforementioned performance determining factors as demonstrated in Fig. 9. To improve the performance of S-CAP in such scenarios, power factor imbalance (PFI) and multiple PDs are employed. Inducing PFI redistributes the transmit power from the LEDs non-uniformly and thereby restoring dissimilarity among the channel gains. The PFI is implemented by scaling the emitted optical power from each LED with a weighting factor, δ_{n_t}. The weighting factor, generated such that the total transmit power is preserved, is given as:

$$\delta_{n_t} = \left(\frac{1}{N_t} \sum_{i=1}^{N_t} 10^{0.1(i-n_t)\zeta} \right)^{-1} \tag{20}$$

where ζ is a user-defined PFI in dB. It should be noted that inducing PFI does not increase the total transmit power nor the detection complexity at the receiver [26]. For example, if $\zeta = 2$ dB in (20), the emitted optical power from LEDs 1 to 4 are scaled by $\delta_1 = 0.4406$, $\delta_2 = 0.6984$, $\delta_3 = 1.1068$ and $\delta_4 = 1.7542$, respectively.

Figures 10 and 11 depict the influence of the two performance-enhancing techniques on the performance of S-CAP LOS propagation at location A and B in Fig. 9, respectively. It is shown that the BER performance can be significantly improved using these techniques. A gain of 30 dB and 33.5 dB can be realised at BER of 10^{-4} using PFI of 1 dB and 2 dB, respectively at location A as shown in Fig. 10. Similarly, at the same location A, the use of multiple PDs

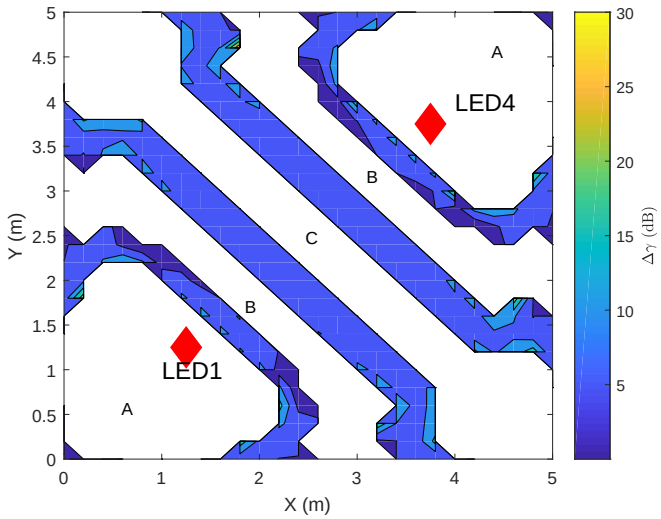

Fig. 13. The γ_b penalty incurred by S-CAP16 to achieve the FEC BER limit of 3×10^{-3} in an optical indoor multipath propagation with second-order reflections in comparison to LOS propagation. The white regions indicate region where BER $> 3 \times 10^{-3}$.

results in performance gain of 3 dB and 43 dB corresponding to two and four PDs, respectively. Using multiple PDs increases the performance since receiving the same symbol in multiple locations increases the probability of correctly detecting that symbol. However, the diversity gain due to multiple PDs is a function of the PD positions. To illustrate this, the use of two PDs at locations $(0.8, 4.2)$ and $(4.2, 0.8)$, both with channel gain of 1, in Fig. 11 lead to no improvement. However, using four PDs significantly reduces the BER to 10^{-4} at an γ_b of 13 dB. Also, Fig 11 shows that the use of 1 dB and 2 dB PFI improve the irreducible BER at location B to 10^{-4} at γ_b of 28 dB and 22 dB, respectively. Therefore, both multiple PDs and PFI are effective in significantly improving the BER performance of S-CAP in indoor LOS propagation.

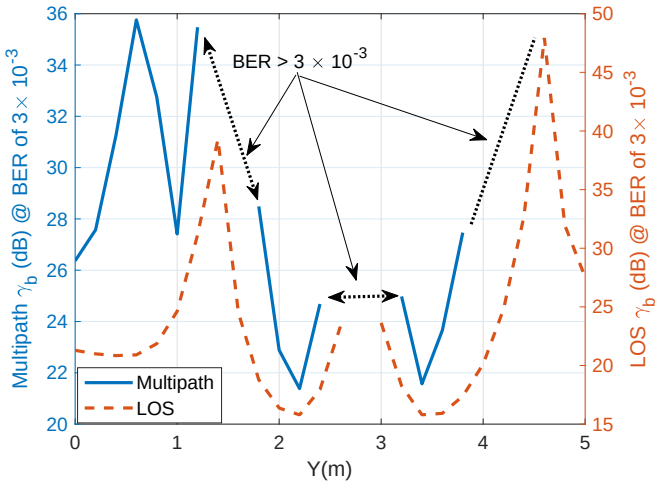

Fig. 14. Comparison of the BER performance trend of S-CAP16 in multipath and LOS propagation across the room for a fixed location on x-axis (x = 2.2 m) and at the FEC BER limit of 3×10^{-3}.

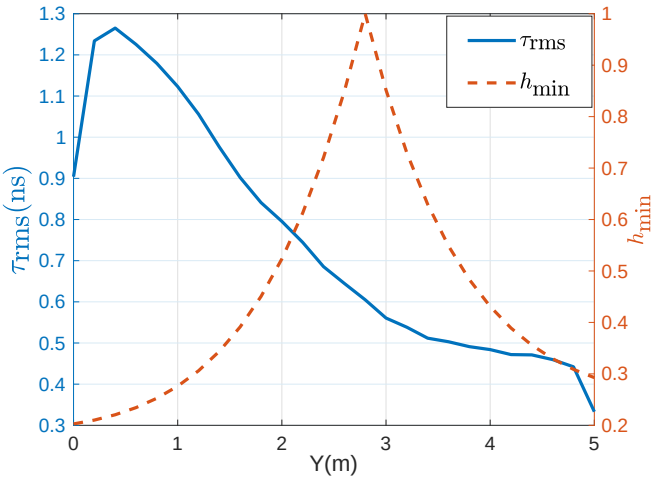

Fig. 15. Comparison of the trend followed by τ_{rms} and $h$min across the room for a fixed location on x-axis (x = 2.2 m).

The majority of the studies on optical spatial modulation have been in LOS indoor propagation [13, 15, 26]. For high-speed indoor optical communication however, the presence of multiple reflections impair the link performance [27–29]. The multiple reflections of the transmitted signal that arrive at the receiver much later than the LOS, though carry much smaller power, can not be ignored due to their time-dispersive properties especially when considering high-speed indoor optical communication. These reflections constitute non-line of sight (NLOS) propagation which reduces the quality of the received signal. Therefore, the performance of S-CAP in multipath indoor optical communication is studied considering CIR with up to second-order multipath reflections. The time-dispersive property of multipath propagation is quantified using the RMS channel delay spread, τ_{rms} defined as [27, p. 85]:

$$\tau_{\text{rms}} = \left[\frac{\int (t-\mu)^2 h^2(t) dt}{\int h^2(t) dt} \right]^{1/2} \tag{21}$$

where μ is the mean delay spread given by :

$$\mu = \frac{\int t h^2(t) dt}{\int h^2(t) dt} \tag{22}$$

The maximum data rate that can be transmitted in a diffuse channel without the need for equalization is given as $R_b \leq 0.1/\tau_{\text{rms}}$ [27, p. 465]. Hence, normalizing the τ_{rms} by bit duration, the maximum normalized τ_{rms} can be obtained as $\bar{\tau}_{\text{rms}} = 0.1$. Therefore, for the multipath study, the range of $0.1 \leq \bar{\tau}_{\text{rms}} \leq 0.4$ is considered across the room.

The impact of indoor multipath propagation with second-order reflections on the BER performance of S-CAP is presented in Fig. 12 at two different locations with $\bar{\tau}_{\text{rms}}$ of 0.4 (PD1) and 0.28 (PD2). At PD1 location where $\bar{\tau}_{\text{rms}} = 0.4$, S-CAP is able to achieve a BER of 10^{-4} with an SNR of 29.5 dB in LOS propagation in comparison to the error floor of 8×10^{-2} it achieved in multipath. Similarly, it reaches error

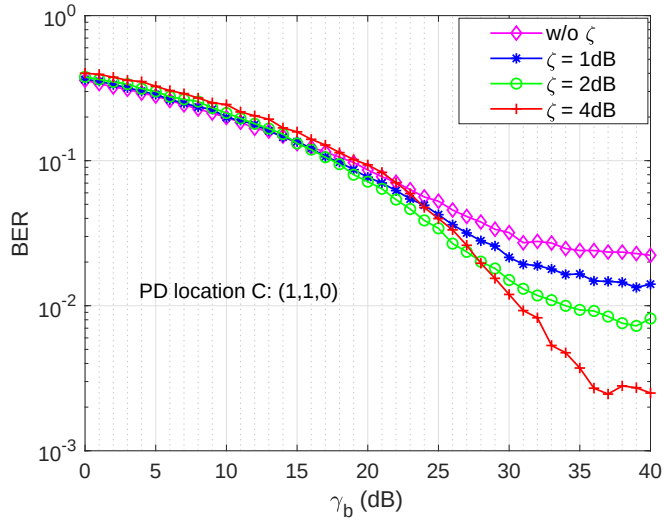

Fig. 16. BER performance improvement for S-CAP16 using PFI in a multipath propagation with second-order reflections at a location dominated by τ_{rms}.

floor of 7×10^{-4} in multipath propagation at PD2 location while it is able to achieve a BER of 10^{-4} in LOS with an SNR of 28.5 dB. This shows the impact of indoor multipath propagation on the BER performance of S-CAP. This figure also indicates that the S-CAP performance in multipath will depend on the particular location in the room hence, the effect of user mobility across the room is further investigated.

The γ_b penalty (Δ_γ) incurred due to the multipath propagation effect in comparison to the LOS scenario is shown in Fig. 13. It is seen that the penalty could be up to 30 dB in γ_b to achieve a BER of 3×10^{-3} in some parts of the room due to the effect of NLOS propagation. The regions marked A, B and C in Fig. 13 correspond to the earlier mentioned three factors influencing S-CAP performance. However, in contrast to the case of LOS where h_{min} is the dominant factor in region A, it is the τ_{rms} that dominates the BER performance in this region in multipath propagation.

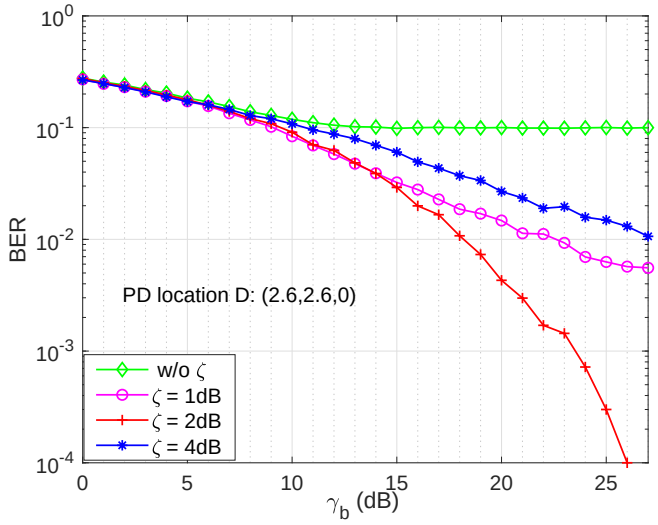

Fig. 17. BER performance improvement for S-CAP16 using PFI in multipath propagation with second-order reflections at a location dominated by $h_{\min}$.

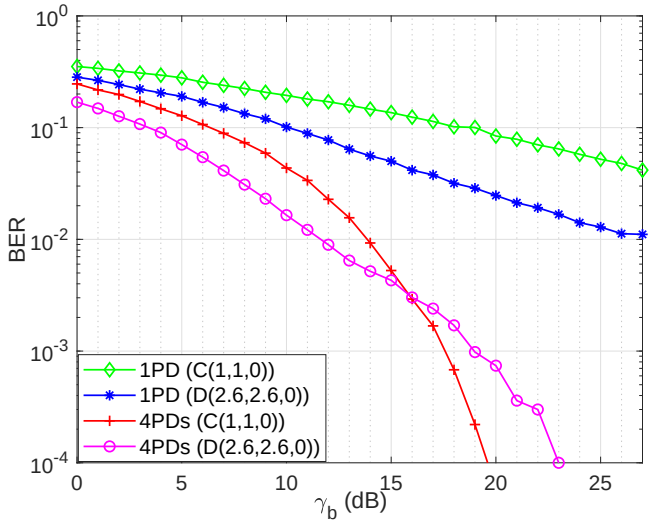

Fig. 18. BER performance improvement for S-CAP16 using multiple PDs in multipath propagation with second-order reflections.

In order to show the influence of these factors, the performance of S-CAP in LOS and multipath propagation is compared and presented in Fig. 14 at the forward error correction (FEC) BER limit of 3×10^{-3} and location $x = 2.2$ m. The corresponding values of $h_{\min}$ and τ_{rms} are shown in Fig. 15. Within the range $0 \leq Y(m) \leq 1$, Fig. 14 shows that the multipath performance follows exactly the trend of τ_{rms} in Figs. 15 while LOS performance follows that of $h_{\min}$. However, between $1 < Y(m) \leq 5$ both the performance of S-CAP in LOS and multipath follow the same trend though the BER in the multipath case is higher. Therefore it can be deduced that while $h_{\min}$, SCP and $|\Delta h|$ dominate S-CAP performance in LOS propagation, it is the τ_{rms}, SCP and $|\Delta h|$ that dictate performance in multipath scenario. This is due to the fact that τ_{rms} overrides the influence of $h_{\min}$ especially where the latter has small values ($0 < h_{\min} < 0.3$) and the former has high values ($0.9 \leq \tau_{\text{rms}} \leq 1.3$).

The results discussed above indicate that the BER performance in multipath propagation can be divided into two regions. The region dominated by the multipath factor, τ_{rms} and the region dominated by LOS factors, SCP and $|\Delta h|$. Hence two locations in Fig. 13, one each from the multipath and LOS region where there is irreducible BER, have been selected in investigating the performance of PFI and multiple PDs in multipath propagation.

The results of the PFI are presented in Figs. 16 and 17. Location C with $\bar{\tau}_{\text{rms}} = 0.31$ and location D with $\bar{\tau}_{\text{rms}} = 0.13$ belong to the multipath and LOS region, respectively and S-CAP performance suffers irreducible error floor at both locations. The PFI is found to be ineffective in improving the BER performance degradation in the region with high τ_{rms} as shown in Fig. 16. However, PFI is able to improve the performance in region dominated by SCP and $|\Delta h|$ to achieve BER of 10^{-4} at γ_b of 28 dB using $\zeta = 2$ dB. This confirms the earlier results regarding the effectiveness of PFI in LOS scenario. It can thus be said that PFI does not significantly improve the BER performance in multipath propagation in the region dominated by high τ_{rms}. Also, it can be deduced from Fig. 17 that the value of PFI should not be too high as $\zeta = 4$ dB results in performance degradation. While PFI increase results by increasing channel gain dissimilarity, it also reduces the emitted optical power on some of the LEDs. This results in low SNR on these LEDs and hence, the consequent degradation in BER performance.

Multiple PDs are also employed to improve performance of S-CAP in multipath channel. The results, as presented in Fig. 18, show that the performance can be significantly improved with the use of multiple PDs. In comparison to the previous irreducible error performance, BER of 10^{-4} is achieved in location C and D at γ_b of 19.5 dB and 23 dB, respectively using 4 PDs. This shows that multiple PDs can be employed to significantly improve the performance of S-CAP in both LOS and multipath propagation.

V. Conclusion

Spatial carrierless amplitude and phase modulation (S-CAP) has been proposed in this work as a low-complexity, spectrally-efficient scheme for visible light communication system. The proposed S-CAP improves the efficiency of the conventional CAP scheme by a factor of $\log_M(MN_{\text{t}})$. An analytical expression for the BER performance of S-CAP in LOS propagation is derived and verified via simulation. It is found that the BER performance of S-CAP in LOS propagation is dictated by the minimum of the channel gains $h_{\min}$, the signal constellation points, SCP and the channel dissimilarity, $\Delta|h|$. While in multipath propagation, the channel delay spread τ_{rms} overrides the influence of $h_{\min}$. The impact of multipath propagation due to second-order reflections on the performance of S-CAP is also reported. Considering user mobility across the room at the FEC BER limit of 3×10^{-3}, multipath propagation results in up to 30 dB SNR penalty in some parts of the room. Both power factor imbalance (PFI) and the use of multiple

photodiode receivers (multiple PDs) are then introduced as performance enhancing techniques. PFI is found to be very effective in improving performance for LOS scenario resulting in SNR gain of 33.5 dB for PFI = 2 dB while it is largely ineffective in multipath scenario when the performance is dominated by high τ_{rms}. In contrast, multiple PDs are able to significantly improve the performance of S-CAP in both LOS and multipath channels leading to 43 dB SNR gain with the use of four PDs.

REFERENCES

[1] D. Karunatilaka, F. Zafar, V. Kalavally, and R. Parthiban, "LED based indoor visible light communications: State of the art," *IEEE Communications Surveys Tutorials*, vol. 17, no. 3, pp. 1649–1678, thirdquarter 2015.

[2] N. Chi, H. Haas, M. Kavehrad, T. D. C. Little, and X. L. Huang, "Visible light communications: demand factors, benefits and opportunities [guest editorial]," *IEEE Wireless Communications*, vol. 22, no. 2, pp. 5–7, April 2015.

[3] "IEEE standard for local and metropolitan area networks–part 15.7: Short-range wireless optical communication using visible light," *IEEE Std 802.15.7-2011*, pp. 1–309, Sept 2011.

[4] *IEEE 802.15 WPAN 15.7 Maintenance: Short-Range Optical Wireless Communications Task Group (TG 7m)*, "IEEE Standards Association" Std. [Online]. Available: "http://www.ieee802.org/15/pub/IEEE 802_15 WPAN 15_7 Revision1 Task Group.htm, accessed April 15 2018"

[5] W. O. Popoola, "Impact of VLC on light emission quality of white LEDs," *Journal of Lightwave Technology*, vol. 34, pp. 2526–2532, 2016.

[6] X. Li *et al.*, "Wireless visible light communications employing feed-forward pre-equalization and PAM-4 modulation," *Journal of Lightwave Technology*, vol. 34, no. 8, pp. 2049–2055, April 2016.

[7] M. S. Islim *et al.*, "Towards 10 Gb/s orthogonal frequency division multiplexing-based visible light communication using a GaN violet micro-LED," *Photon. Res.*, vol. 5, no. 2, pp. A35–A43, Apr 2017.

[8] Y. Wang, L. Tao, X. Huang, J. Shi, and N. Chi, "8-Gb/s RGBY LED-based WDM VLC system employing high-order CAP modulation and hybrid post equalizer," *IEEE Photonics Journal*, vol. 7, no. 6, pp. 1–7, Dec 2015.

[9] P. A. Haigh *et al.*, "Multi-band carrier-less amplitude and phase modulation for bandlimited visible light communications systems," *IEEE Wireless Communications*, vol. 22, no. 2, pp. 46–53, April 2015.

[10] P. A. Haigh *et al.*, "A multi-CAP visible-light communications system with 4.85-b/s/Hz spectral efficiency," *IEEE Journal on Selected Areas in Communications*, vol. 33, no. 9, pp. 1771–1779, Sept 2015.

[11] P. Chvojka *et al.*, "On the m-CAP performance with different pulse shaping filters parameters for visible light communications," *IEEE Photonics Journal*, vol. 9, no. 5, pp. 1–12, Oct 2017.

[12] Y. Wang, L. Tao, Y. Wang, and N. Chi, "High speed WDM VLC system based on multi-band CAP-64 with weighted pre-equalization and modified CMMA based post-equalization," *IEEE Communications Letters*, vol. 18, no. 10, pp. 1719–1722, Oct 2014.

[13] W. O. Popoola, E. Poves, and H. Haas, "Error performance of generalised space shift keying for indoor visible light communications," *IEEE Transactions on Communications*, vol. 61, no. 5, pp. 1968–1976, 2013.

[14] W. O. Popoola and H. Haas, "Demonstration of the merit and limitation of generalised space shift keying for indoor visible light communications," *Journal of Lightwave Technology*, vol. 32, no. 10, pp. 1960–1965, May 2014.

[15] W. O. Popoola, E. Poves, and H. Haas, "Spatial pulse position modulation for optical communications," *Journal of Lightwave Technology*, vol. 30, no. 18, pp. 2948–2954, Sept 2012.

[16] K. Werfli *et al.*, "Experimental demonstration of high-speed 4×4 imaging multi-CAP MIMO visible light communications," *Journal of Lightwave Technology*, vol. 36, no. 10, pp. 1944–1951, May 2018.

[17] K. O. Akande and W. O. Popoola, "MIMO techniques for carrierless amplitude and phase modulation in visible light communication," *IEEE Communications Letters*, vol. PP, no. 99, pp. 1–1, 2018.

[18] M. D. Renzo, H. Haas, A. Ghrayeb, S. Sugiura, and L. Hanzo, "Spatial modulation for generalized MIMO: Challenges, opportunities, and implementation," *Proceedings of the IEEE*, vol. 102, no. 1, pp. 56–103, Jan 2014.

[19] X. Zhang, S. Dimitrov, S. Sinanovic, and H. Haas, "Optimal power allocation in spatial modulation OFDM for visible light communications," in *2012 IEEE 75th Vehicular Technology Conference (VTC Spring)*, May 2012, pp. 1–5.

[20] J. Jeganathan, A. Ghrayeb, and L. Szczecinski, "Spatial modulation: optimal detection and performance analysis," *IEEE Communications Letters*, vol. 12, no. 8, pp. 545–547, Aug 2008.

[21] H. G. Olanrewaju, J. Thompson, and W. O. Popoola, "On spatial pulse position modulation for optical wireless communications," in *2016 IEEE Photonics Society Summer Topical Meeting Series (SUM)*, July 2016, pp. 44–45.

[22] J. G. Proakis, *Digital Communications, (4th Ed)*. New York: McGraw-Hill, 2001.

[23] J. R. Barry, J. M. Kahn, W. J. Krause, E. A. Lee, and D. G. Messerschmitt, "Simulation of multipath impulse response for indoor wireless optical channels," *IEEE Journal on Selected Areas in Communications*, vol. 11, no. 3, pp. 367–379, Apr 1993.

[24] J. M. Kahn and J. R. Barry, "Wireless infrared communications," *Proceedings of the IEEE*, vol. 85, no. 2, pp. 265–298, Feb 1997.

[25] K. Lee, H. Park, and J. R. Barry, "Indoor channel characteristics for visible light communications," *IEEE Communications Letters*, vol. 15, no. 2, pp. 217–219, February 2011.

[26] T. Fath and H. Haas, "Performance comparison of MIMO techniques for optical wireless communications in indoor environments," *IEEE Transactions on Communications*, vol. 61, no. 2, pp. 733–742, 2013.

[27] Z. Ghassemlooy, W. Popoola, and S. Rajbhandari, *Optical Wireless Communications: System and Channel Modelling with MATLAB*, 1st ed. Boca Raton, FL, USA: CRC Press, Inc., 2012.

[28] M. D. Audeh, J. M. Kahn, and J. R. Barry, "Performance of pulse-position modulation on measured non-directed indoor infrared channels," *IEEE Transactions on Communications*, vol. 44, no. 6, pp. 654–659, 1996.

[29] J. B. Carruthers and J. M. Kahn, "Modeling of nondirected wireless infrared channels," *IEEE Transactions on Communications*, vol. 45, no. 10, Oct 1997.